Applied Catalysis B: Environmental 150–151 (2014) 187–196

Contents lists available at ScienceDirect

Applied Catalysis B: Environmental

journal homepage: www.elsevier.com/locate/apcatb

# Hydrothermal-synthesized $SrTiO_3$ photocatalyst codoped with rhodium and antimony with visible-light response for sacrificial $H_2$ and $O_2$ evolution and application to overall water splitting

Ryo Niishiro[a], Shumpei Tanaka[a], Akihiko Kudo[a,b,*]

[a] Department of Applied Chemistry, Faculty of Science, Tokyo University of Science , 1-3 Kagurazaka, Shinjuku-ku, Tokyo 162-8601, Japan
[b] Photocatalysis International Research Center, Research Institute for Science and Technology, Tokyo University of Science , 2641 Yamazaki, Noda-shi, Chiba 278-8510, Japan

ARTICLE INFO

*Article history:*
Received 18 August 2013
Received in revised form 2 December 2013
Accepted 8 December 2013
Available online 14 December 2013

*Keywords:*
Photocatalyst
Hydrothermal synthesis
Codoping
Water splitting
Visible light

ABSTRACT

The codoping effect of antimony on the photocatalytic activity of visible-light-driven $SrTiO_3$ doped with rhodium ($SrTiO_3$:Rh) was investigated. $SrTiO_3$ doped with rhodium and antimony ($SrTiO_3$:Rh/Sb) prepared by a hydrothermal method was found to be active for photocatalytic $H_2$ evolution from an aqueous methanol solution and $O_2$ evolution from an aqueous silver nitrate solution under visible light irradiation, although $SrTiO_3$ doped with rhodium and no antimony was active only for the $H_2$ evolution. Photocatalytic activities of $SrTiO_3$:Rh/Sb were strongly dependent on the ratio of codopant to dopant (Sb/Rh). Diffuse reflection spectroscopy (DRS), electron spin resonance (ESR), Raman, and action spectrum analyses revealed the contribution of rhodium and antimony to visible-light response of $SrTiO_3$:Rh/Sb. Unstable and reversible $Rh^{3+}$ ions in oxidation state were the superior species for the $H_2$ evolution. On the other hand, $Rh^{3+}$ ions stabilized by codoping of antimony without the formation of $Rh^{4+}$ ions and oxygen defects which would work as undesirable recombination sites between photogenerated electrons and holes played an important role in the $O_2$ evolution. Moreover, when an $IrO_X$ cocatalyst was loaded on the surface of the $SrTiO_3$:Rh/Sb photocatalyst, the photocatalytic activity of the $O_2$ evolution drastically increased. The apparent quantum yield for the $H_2$ evolution over Pt(0.3 wt%)/$SrTiO_3$:Rh(1%)/Sb(1%) and the $O_2$ evolution over $IrO_X$(3.0 wt%)/$SrTiO_3$:Rh(1%)/Sb(1%) at 420 nm were 0.8% and 4.5%, respectively. The *Z*-scheme system composed of Ru(1.0 wt%)/$SrTiO_3$:Rh(2%) as a $H_2$-evolving photocatalyst, $IrO_X$(3.0 wt%)/$SrTiO_3$:Rh(1%)/Sb(1%) as an $O_2$-evolving photocatalyst, and an $Fe^{3+}/Fe^{2+}$ redox couple as an electron mediator showed photocatalytic activity for overall water splitting under visible light irradiation.



## 1. Introduction

Overall water splitting using semiconductor photocatalysts has been studied extensively from the viewpoint of solar energy conversion [1–5]. In order to utilize sunlight efficiently, the development of visible-light responsive photocatalyst materials is indispensable. Some photocatalysts with visible-light response for overall water splitting have been developed [6–14]. However, their quantum yields are not sufficient as compared with those of UV-light-responsive photocatalysts.

There are many photocatalysts with visible-light response for $H_2$ or $O_2$ evolution from aqueous solutions containing sacrificial regents [15–37]. Doping of foreign elements can sensitize wide band gap photocatalysts to visible light. The present authors have developed some visible-light-driven ZnS [19,20,25], $TiO_2$ [21,29,30], $SrTiO_3$ [21,27–29], $PbMoO_4$ [31], $NaMO_3$ (M = Nb and Ta) [32], and $K_2LaNb_5O_{15}$ [35] photocatalysts doped with metal cations. However, metal cation-doped materials usually show photocatalytic activity for either the $H_2$ or $O_2$ evolution. In order to achieve overall water splitting under visible light irradiation by use of a single photocatalyst, the photocatalyst has to possess abilities for $H_2$ and $O_2$ evolution.

Rhodium-doped $SrTiO_3$ ($SrTiO_3$:Rh) shows the high photocatalytic activity for the $H_2$ evolution from an aqueous methanol solution under visible light irradiation among visible-light-driven oxide photocatalysts [28]. The present authors suggested that rhodium species with reversibility in oxidation state contributed to the visible-light response. However, the $SrTiO_3$ doped with rhodium cannot oxidize water to $O_2$ even in the presence of $Ag^+$ as an electron acceptor. On the other hand, $TiO_2$ photocatalysts codoped with chromium and antimony ($TiO_2$:Cr/Sb) [21], and rhodium and antimony ($TiO_2$:Rh/Sb) [30] show photocatalytic

* Corresponding author. Tel.: +81 3 5228 8267; fax: +81 3 5261 4631.
*E-mail address:* a-kudo@rs.kagu.tus.ac.jp (A. Kudo).

0926-3373/$ – see front matter © 2013 Elsevier B.V. All rights reserved.
http://dx.doi.org/10.1016/j.apcatb.2013.12.015

activity for the $O_2$ evolution although their activities for the $H_2$ evolution are negligible probably because of their low conduction band levels. These studies indicate that the control of oxidation state of dopant cations by codoping of antimony is a key issue. The codoping that contributes to keeping charge balance suppresses the formation of undesirable species such as $Cr^{6+}$, $Rh^{4+}$, and oxygen defects which work as recombination centers between photogenerated electrons and holes. It results in giving visible-light response of $TiO_2$ photocatalysts for the $O_2$ evolution from an aqueous silver nitrate solution. Therefore, it is expected that visible-light response for the $O_2$ evolution should appear for the rhodium–doped $SrTiO_3$ photocatalyst, if the oxidation state of doped rhodium cations is controllable by the codoping technique.

Photocatalytic activities of powdered semiconductor materials are dependent on the preparation methods. The photocatalytic activities for water splitting by $NaTaO_3$ [38], $Sr_2Ta_2O_7$ [39], $Ba_5Nb_4O_{15}$ [40] and for the $O_2$ evolution by $BiVO_4$ [41,42] prepared by aqueous processes are higher than those prepared by solid-state reactions mainly due to the improvements in morphology, particle sizes, and crystallinities. On the other hand, $SrTiO_3$ photocatalysts codoped with chromium and tantalum ($SrTiO_3$:Cr/Ta) [27], and nickel and tantalum ($SrTiO_3$:Ni/Ta) [29] show activities for $H_2$ evolution from an aqueous methanol solution under visible light irradiation. Although charge compensation by codoping of $Ta^{5+}$ is effective in photocatalytic activities of $SrTiO_3$:Cr/Ta and $SrTiO_3$:Ni/Ta prepared by solid-state reactions, the formation of undesirable $Cr^{6+}$ and $Ni^{3+}$ with high-valent state cannot be suppressed completely. In the case of codoping-type materials, homogeneity of dopant and codopant cations in host materials is important from the viewpoint of charge compensation. As aqueous processes should provide higher homogeneity of dopant and codopant cations than a solid-state reaction in preparation, it is expected that preparation of aqueous processes improves the efficiency of charge compensation in codoped photocatalyst.

In the present study, codoping of antimony was applied to $SrTiO_3$:Rh by a hydrothermal method in order to give new photocatalytic ability. Photocatalytic activities of rhodium and antimony-codoped $SrTiO_3$ ($SrTiO_3$:Rh/Sb) were investigated for $H_2$ and $O_2$ evolutions from aqueous solutions containing sacrificial reagents under visible light irradiation. Effects of antimony codoping on the oxidation state of rhodium cations doped in $SrTiO_3$ and photocatalytic activities of the codoped $SrTiO_3$ were discussed. Water splitting into $H_2$ and $O_2$ under visible light irradiation was demonstrated using a *Z*-scheme system composed of the $SrTiO_3$:Rh/Sb photocatalysts.

## 2. Experimental

### 2.1. Preparation of $SrTiO_3$:Rh/Sb photocatalyst powder

$SrTiO_3$ powder codoped with rhodium and antimony was prepared from $Sr(OH)_2{\cdot}8H_2O$ (High Purity Chemicals; 99%), $TiO_2$ (Nippon Aerosil; P 25), $Rh(NO_3)_3$ (Kanto Chemical), and $Sb_2O_5$ (High Purity Chemicals; 99.9%) by a hydrothermal method in the following manner. The starting materials were added into 50 mL of pure water in a Teflon crucible in the ratio according to the composition of $SrTi_{1-X-Y}Rh_XSb_YO_3$. The Teflon crucible containing the starting materials was placed in an autoclave and then heated at 433 K for 40 h. After cooling to 343 K, the obtained precursor was washed using pure water by centrifuge separation for three times and dried at 333 K for 1 day in air. The obtained precursor powder was calcined at 1273 K for 10 h in air using an alumina crucible. For comparison, a $SrTiO_3$ powder codoped with rhodium and antimony was prepared from $SrCO_3$ (Kanto Chemical; 99.9%), $TiO_2$ (Soekawa Chemical; 99.9%), $Rh_2O_3$ (Wako Pure Chemical; 99.5%), and $Sb_2O_3$ (Nacalai Tesque; 98%) by a solid-state reaction at 1273 K for 10 h in air. $H_2$ reduction at 673 K for 2 h was carried out for some samples in order to reduce $Rh^{4+}$ to $Rh^{3+}$ ions because a part of rhodium cations doped into the $SrTiO_3$ host was oxidized to $Rh^{4+}$ ions during the high-temperature calcination in air. Pt and Ru cocatalysts were loaded from aqueous $H_2PtCl_6{\cdot}6H_2O$ (Tanaka Kikinzoku; 37.55% as Pt) and $RuCl_3{\cdot}nH_2O$ (Wako Pure Chemical; 99.9%) solutions containing 10 vol% of methanol by a photodeposition method. $IrO_X$ cocatalysts were loaded by adsorption of colloidal $IrO_X$ prepared from $K_2IrCl_6$ (Wako Pure Chemical; 38.8–40.8% as Ir) [22], and then heated at 623 K for 1 h in air except for the sample reduced with $H_2$.

### 2.2. Characterization of photocatalyst

Crystal phases of the obtained powders were confirmed by X-ray diffraction (Rigaku; MiniFlex, Cu $K\alpha$). The X-ray diffraction (XRD) patterns were collected from 5° to 70° ($2\theta$) by use of a step size of 0.02°. The source power and current of Cu $K\alpha$ radiation were 30 kV and 10 mA, respectively. Diffuse reflection spectra (DRS) were obtained by use of a UV–VIS–NIR spectrometer (Jasco; UbestV-570) and were converted from reflectance to absorbance by the Kubelka–Munk method. Raman spectra were obtained using a Raman spectrometer (Jasco; NRS-3200). The XRD, DRS, and Raman measurements were carried out at room temperature. X-band electron spin resonance (ESR) measurements (JEOL; JES-FA200) were carried out at 77 K in vacuo using flame-sealed ESR tubes made of quartz (microwave frequency, 9.13 GHz; microwave power, 1.0 mW; modulation frequency, 100 kHz).

### 2.3. Photocatalytic reactions

Photocatalytic reactions for $H_2$ evolution from an aqueous methanol solution (10 vol%), $O_2$ evolution from an aqueous silver nitrate solution (0.02 mol $L^{-1}$), and water splitting were carried out in a gas-closed circulation system. Argon gas (20 Torr) was introduced into the system after deaeration. The photocatalyst powder (0.05–0.2 g) was dispersed in the reactant solution (120–150 mL) by a magnetic stirrer in a cell with a top window made of Pyrex. A300-W Xe lamp (Perkin-Elmer; CERMAX-PE300F) attached with a cutoff filter (HOYA; L42) was employed for visible light irradiation. The amounts of evolved $H_2$ and $O_2$ were determined by use of on-line gas chromatography (Shimazu; GC-8A, MS-5A column, TCD, Ar carrier). Apparent quantum yields were measured using a Xe lamp (Asahi Spectra; MAX-301) and band-pass filters (Asahi Spectra; MX0420–0600) for irradiating monochromatic lights. A photodiode (OPHIR; PD300-UV SH head and NOVA display) was used for the measurement of the number of incident photons. Apparent quantum yields were determined by the following equation:Apparent quantum yield (%)

=the number of reacted electrons or holes/the number of incident photons × 100;

=the number of $H_2$ molecules × 2/the number of incident photons × 100 (for $H_2$ evolution);

=the number of $O_2$ molecules × 4/the number of incident photons × 100 (for $O_2$ evolution).

## 3. Results and discussion

### 3.1. Effects of antimony codoping on oxidation state of doped rhodium and photoabsorption property of $SrTiO_3$:Rh/Sb

XRD analyses revealed that all samples had a single phase of $SrTiO_3$ (see Supplementary data Fig. S1). Here, the amount of doped rhodium was fixed at 2% ($SrTiO_3$:Rh(2%)/Sb(Y%)). No impurity phases were observed. Crystallinities of calcined $SrTiO_3$:Rh/Sb

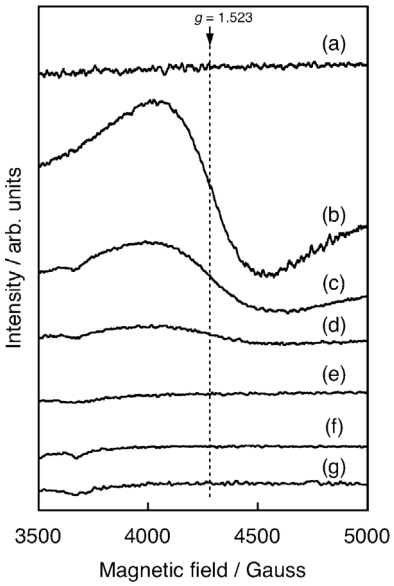


**Fig. 1.** ESR spectra measured at 77 K in vacuo of (a) non-calcined $SrTiO_3$:Rh and calcined $SrTiO_3$:Rh/Sb with Sb/Rh ratios: (b) 0; (c) 0.5; (d) 1.0; (e) 1.5; and (f) $SrTiO_3$:Rh treated with $H_2$ at 673 K for 2 h, and (g) $SrTiO_3$:Sb(2%). The amount of doped Rh was fixed at 2%.

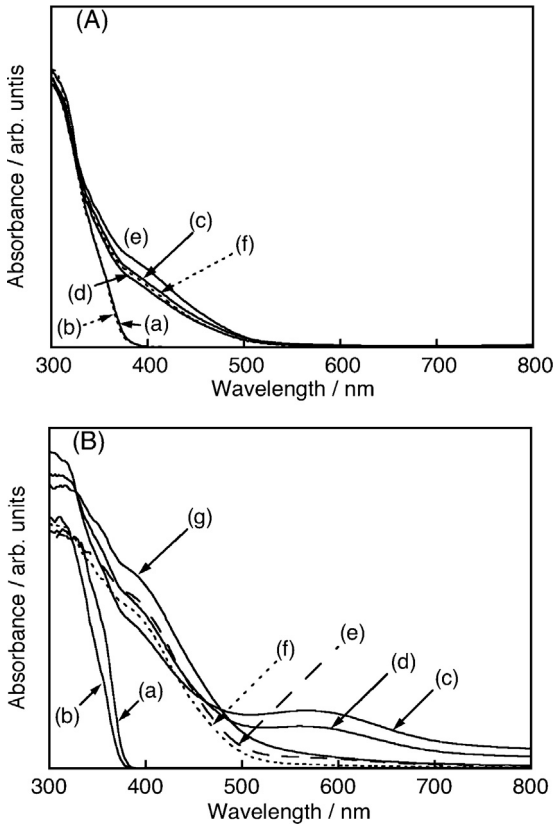


**Fig. 2.** Diffuse reflection spectra of (A) non-calcined and (B) calcined $SrTiO_3$:Rh/Sb. (a) non-doped $SrTiO_3$, (b) $SrTiO_3$:Sb(2%), and $SrTiO_3$:Rh/Sb with Sb/Rh ratios: (c) 0; (d) 0.5; (e) 1.0; (f) 1.5; and (g) $SrTiO_3$:Rh treated with $H_2$ at 673 K for 2 h. The amount of doped Rh was fixed at 2%.

powders were higher than those of non-calcined samples. The crystallinity of the calcined samples obtained by the hydrothermal synthesis was similar to that by the sample obtained by a solid-state reaction.

Fig. 1 shows ESR spectra of $SrTiO_3$:Rh(2%)/Sb(Y%). No signals were observed for non-calcined $SrTiO_3$:Rh without Sb-codoping. In contrast, broad ESR signals were observed in $SrTiO_3$:Rh/Sb (Sb/Rh = 0, 0.5, and 1.0). $Rh^{3+}$ and $Rh^{4+}$ are stable cations in oxides. $Rh^{3+}$ is diamagnetic and cannot be observed by ESR. Therefore, the observed signals would be related to $Rh^{4+}$. It was reasonable from the viewpoint of charge balance that a part of $Rh^{3+}$ ion substituted for $Ti^{4+}$ sites in the lattice of $SrTiO_3$ host was oxidized to $Rh^{4+}$ ion by high-temperature calcination in air. When $SrTiO_3$:Rh/Sb was reduced with $H_2$, $Rh^{4+}$ ions were reduced to $Rh^{3+}$, resulting in the disappearance of the signal. On the other hand, the ESR signal related to $Rh^{4+}$ ions weakened gradually with increasing the amount of codoped antimony. When the Sb/Rh ratio was 1.5, the signal disappeared and almost the same spectrum as $SrTiO_3$ doped with only antimony was obtained. This was due to the charge compensation by codoped $Sb^{5+}$ ions to form $Rh^{3+}$ ions stabilized against oxidation by high-temperature calcination in air, resulting in the suppression of the $Rh^{4+}$ formation. The stoichiometric ratio between $Sb^{5+}$ and $Rh^{3+}$ at $Ti^{4+}$ sites should be unity from the viewpoint of charge balance. When the Sb/Rh ratio was 0.5, the amount of codoped antimony was not enough intrinsically. A weak ESR signal related to $Rh^{4+}$ ions was detected even for the sample with Sb/Rh = 1.0. In contrast, the complete charge compensation was achieved in the sample with Sb/Rh = 1.5. This charge compensation effect is similar to that for $TiO_2$:Cr/Sb and $TiO_2$:Rh/Sb [21,30].

Fig. 2 shows DRS of $SrTiO_3$:Rh(2%)/Sb(Y%). The onset of the intrinsic band gap absorption of $SrTiO_3$ doped with only antimony (Fig. 2(A)b and (B)b) almost corresponded with that of non-doped $SrTiO_3$ (Fig. 2(A)a and (B)a). This observation showed that the effect of doped antimony on the band position of the $SrTiO_3$ host was negligible. All of non-calcined $SrTiO_3$:Rh/Sb with different Sb/Rh ratios had visible light absorption bands in addition to their intrinsic band gap absorption bands (Fig. 2(A)c–f). Profiles of these visible light absorption bands were changed by high-temperature calcination in air (Fig. 2(B)c–f). The calcined sample with Sb/Rh = 0 (Fig. 2(B)c) showed some visible light absorption bands which were similar to those of $SrTiO_3$:Rh prepared by a solid-state reaction [28]. An absorption peak around 580 nm disappeared with $H_2$ reduction treatment, while an absorption band with an onset at 530 nm appeared. The tailing beyond 530 nm of the onset was probably due to oxygen defects. On the other hand, codoping of antimony also weakened the intensity of the absorption peak around 580 nm. The more the amount of codoped antimony was, the weaker the absorption band was. The absorption band around 580 nm almost disappeared in the sample with Sb/Rh = 1.5 (Fig. 2(B)f). In contrast, the absorption band around 580 nm of the solid-state synthesized sample still remained even in the Sb/Rh = 3 (see Supplementary data Fig. S2). The color of the $SrTiO_3$:Rh/Sb powder was also changed drastically from gray (Sb/Rh = 0) to clear yellow (Sb/Rh = 1.5) (see Supplementary data Fig. S3). The absorption band around 580 nm and the ESR signal related to $Rh^{4+}$ ions simultaneously weakened with increasing the amount of codoped antimony, and they disappeared at Sb/Rh = 1.5 as shown in Figs. 1 and 2. On the other hand, non-calcined $SrTiO_3$:Rh that did not give an ESR signal related to $Rh^{4+}$ possessed only the visible light absorption band with an onset at 530 nm. These results concluded that the additional visible light absorption with the onset around 530 nm was due to the electronic transition from the electron donor levels consisting of $Rh^{3+}$ 4d orbitals to the conduction band, while the absorption peak around 580 nm was due to the transition from the valence band to the electron acceptor levels consisting of $Rh^{4+}$ 4d orbitals, as discussed in literature [28]. This electronic structure was also confirmed by X-ray emission spectroscopy, X-ray absorption spectroscopy, and first-principles calculation [43]. Thus, codoping of antimony can control the ratio of $Rh^{3+}$ to $Rh^{4+}$ ions which contributed to the visible light absorption as shown in Fig. 3.

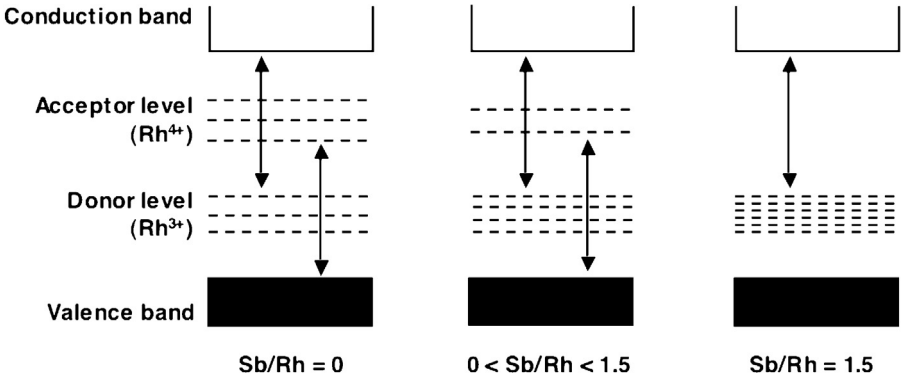


**Fig. 3.** Control of the ratio of $Rh^{3+}$ to $Rh^{4+}$ in $SrTiO_3$:Rh/Sb photocatalysts by codoping of antimony.

Fig. 4 shows Raman spectra of $SrTiO_3$:Rh(2%)/Sb(Y%). The band that was not observed for non-doped $SrTiO_3$ [44] was observed around 800 $cm^{-1}$ in non-calcined and calcined $SrTiO_3$ doped with Rh and/or Sb. It has been reported that the Raman band around 800–900 $cm^{-1}$ is generally observed for complex perovskite materials $AB_ZB'_{1-Z}O_3$ due to ordered distribution of metal cations on the B-site (local short-range order) [45]. This result indicated that rhodium and

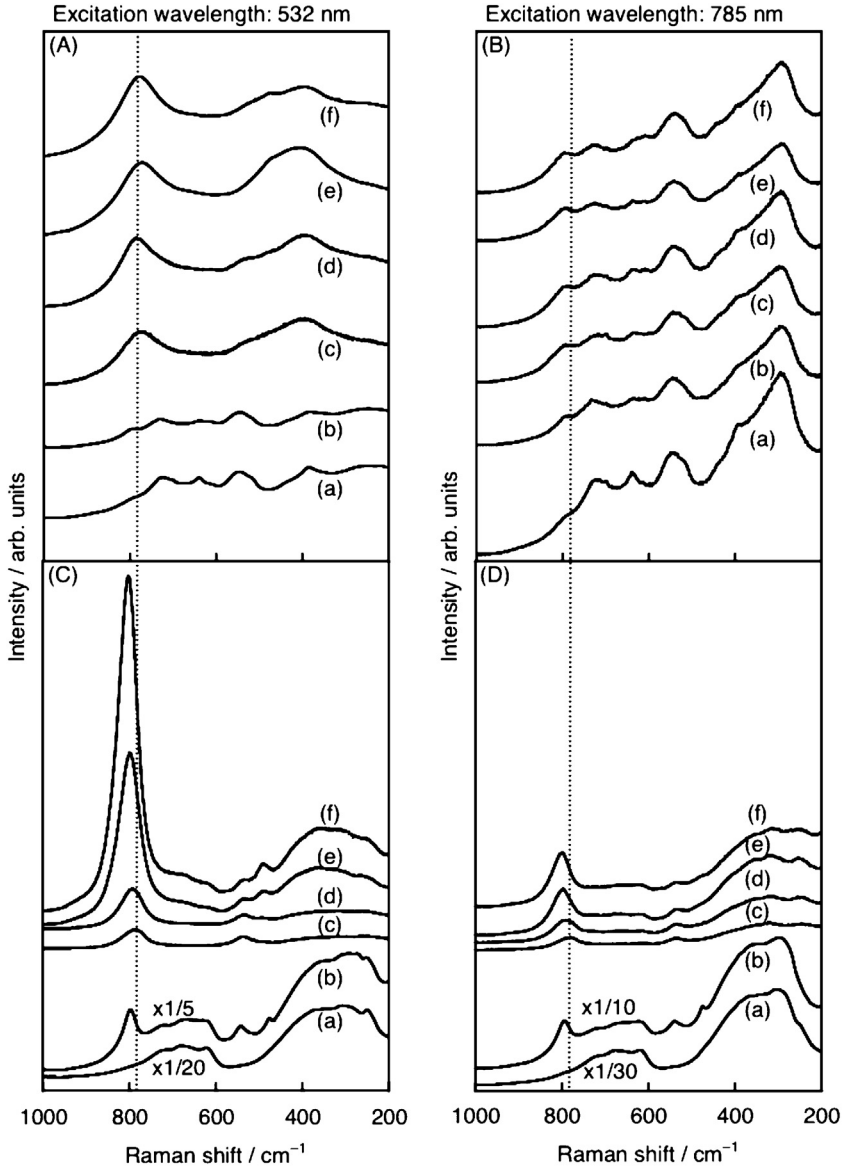


**Fig. 4.** Raman spectra of (A–B) non-calcined and (C–D) calcined $SrTiO_3$:Rh/Sb. (a) non-doped $SrTiO_3$, (b) $SrTiO_3$:Sb(2%), and $SrTiO_3$:Rh/Sb with Sb/Rh ratios: (c) 0; (d) 0.5; (e) 1.0; and (f) 1.5. The amount of doped Rh was fixed at 2%.

antimony cations were substituted for $Ti^{4+}$ sites of the B-site even in the crystal lattice of non-calcined $SrTiO_3$ host. In the cases of calcined samples with high crystallinities, the band intensity around 800 $cm^{-1}$ drastically increased with excitation at 532 nm (Fig. 4(C)c–f) compared with 785 nm (Fig. 4(D)c–f) for codoped $SrTiO_3$. It was also confirmed by comparison of the band intensity around 800 $cm^{-1}$ with the broad band around 200–500 $cm^{-1}$. Such enhancement in the intensity was not observed for $SrTiO_3$ doped with only antimony because the intensity of the band around 800 $cm^{-1}$ was smaller than that around 200–500 $cm^{-1}$. Judging from DRS, the enhancement of the Raman band intensity around 800 $cm^{-1}$ is due to a resonance Raman effect by contribution of the electronic transition from the electron donor levels consisting of $Rh^{3+}$ ions to the conduction band of $SrTiO_3$ with irradiation of 532-nm light. The band around 800 $cm^{-1}$ represents the vibration mode of the local structure around $Rh^{3+}$ ions. Moreover, the codoping of antimony affected the position and intensity for the band around 800 $cm^{-1}$ in $SrTiO_3$:Rh/Sb. The band shifted to higher wavenumber and the intensity became stronger with the increase in the Sb/Rh ratio. This result indicated the interaction between codoped $Rh^{3+}$ and $Sb^{5+}$ due to formation of dopant-codopant pairs. The formation of $SbO_6$ octahedra surrounding $Rh^{3+}$ ions should disturb the symmetry of $RhO_6$ octahedra because antimony is different from titanium in the ionic radius [46] and oxidation state. It resulted in the change in the position and intensity of the Raman band around 800 $cm^{-1}$. The observation of new bands around 476–491 and 537–542 $cm^{-1}$ that were not observed for non-doped $SrTiO_3$ also indicated a decrease in the crystal symmetry in the $SrTiO_3$ host due to the substitution of dopant and codopant for a part of $Ti^{4+}$ sites in the lattice [47]. Such resonance Raman effect and the formation of dopant–codopant pair have also been observed for visible-light-sensitized $TiO_2$:Cr/Sb photocatalysts [48].

The stability of $Rh^{3+}$ ions toward oxidation was efficiently increased by charge compensation, resulting in the complete suppression of the $Rh^{4+}$ formation in the sample with the Sb/Rh = 1.5. In the cases of not only $SrTiO_3$:Rh/Sb but also $SrTiO_3$:Cr/Ta [27] and $SrTiO_3$:Ni/Ta [29] prepared by solid-state reactions, it was impossible to suppress completely the formation of high-valent $Rh^{4+}$, $Cr^{6+}$ and $Ni^{3+}$ ions by only codoping of antimony or tantalum. In the present study, the efficient charge compensation was achieved well by a hydrothermal synthesis compared with the solid-state reaction. If the doping was not homogeneous, systematic changes in DRS, Raman and ESR should not have been observed.

### 3.2. Photocatalytic $H_2$ and $O_2$ evolution from aqueous solutions over $SrTiO_3$:Rh/Sb under visible-light irradiation

Fig. 5 shows photocatalytic $H_2$ evolution from an aqueous methanol solution and $O_2$ evolution from an aqueous silver nitrate solution over Pt- or $IrO_X$-loaded $SrTiO_3$:Rh/Sb with Sb/Rh = 0 and 1.0 under visible light irradiation. The samples with Sb/Rh = 0 and 1.0 evolved $H_2$ steadily after induction periods. In contrast, the sample with Sb/Rh = 0 showed no photocatalytic activity for the $O_2$ evolution. However, when this sample was treated with $H_2$ at 673 K for 2 h and then its surface was modified by loading of $IrO_X$ cocatalyst [22,49,50] which works as an effective $O_2$ evolution site, the activity for the $O_2$ evolution appeared. $IrO_X$-loaded sample with Sb/Rh = 1.0 showed much higher activity for the $O_2$ evolution than that with Sb/Rh = 0 treated with $H_2$. When the amounts of doped rhodium and $IrO_X$ cocatalyst were optimized at 1% (Sb/Rh = 1.0) and 3.0 wt%, respectively, the highest activity was obtained. The decrease in the activity for the $H_2$ evolution with a reaction time is due to the accumulation of $H_2$ that causes poisoning an active site or a reaction with holes [28]. The decrease in the activity for the

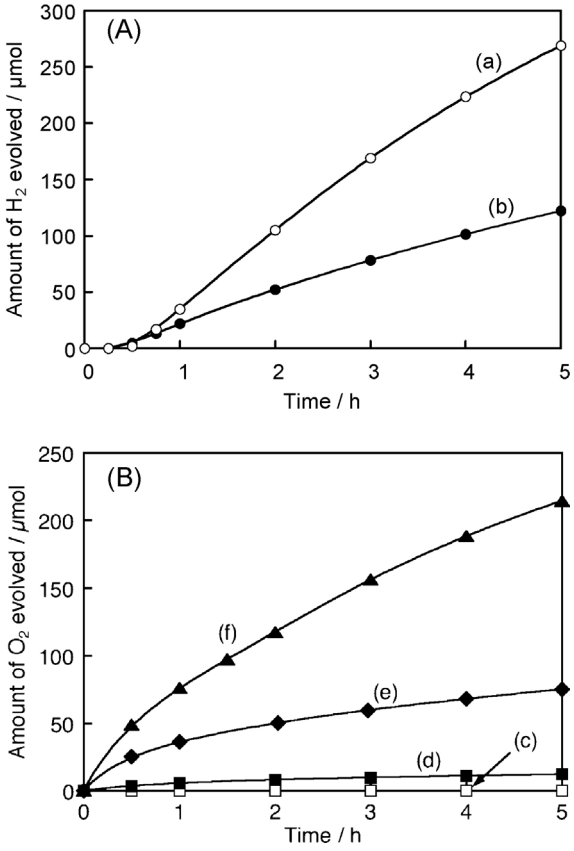


**Fig. 5.** (A) Photocatalytic $H_2$ evolution from 10 vol% aqueous methanol solution over (a) Pt(0.3 wt%)/$SrTiO_3$:Rh(2%) and (b) Pt(0.3 wt%)/$SrTiO_3$:Rh(2%)/Sb(2%). (B) Photocatalytic $O_2$ evolution from 0.02 mol $L^{-1}$ aqueous silver nitrate solution over (c) $SrTiO_3$:Rh(2%), (d) $IrO_X$(1.0 wt%)/$SrTiO_3$:Rh(2%) reduced with $H_2$ at 673 K for 2 h, (e) $IrO_X$ (1.0 wt%)/$SrTiO_3$:Rh(2%)/Sb(2%), and (f) $IrO_X$(3.0 wt%)/$SrTiO_3$:Rh(1%)/Sb(1%). Catalyst, 0.2 g; reactant solution, 150 mL; cell, top-irradiation type; light source, 300-W Xe lamp attached with cutoff filter; incident light, λ > 420 nm.

$O_2$ evolution with a reaction time is due to deposition of metallic Ag that covers the surface and shields incident light [30]. It was interesting that $IrO_X$/$SrTiO_3$:Rh/Sb showed a quite high activity for $O_2$ evolution even if it is a doping photocatalyst [4]. The activity of the sample prepared by a conventional solid state reaction was much lower than that of the present sample indicating the advantage of the hydrothermal synthesis (see Supplementary data Fig. S4). The turnover numbers for the reacted electrons to the amounts of doped rhodium ions at 5 h of the $H_2$ evolution reaction using 0.2 g of $SrTiO_3$:Rh(2%)/Sb(2%) photocatalyst (Fig. 5(A)b) and the $O_2$ evolution reaction using 0.2 g of $SrTiO_3$:Rh(1%)/Sb(1%) photocatalyst (Fig. 5(B)f) reached 11 and 40, respectively. This result proved that both of the $H_2$ and $O_2$ evolutions proceeded photocatalytically under visible light irradiation. Thus, codoping of antimony activated rhodium-doped $SrTiO_3$ photocatalyst for $O_2$ evolution from an aqueous silver nitrate solution under visible light irradiation with keeping the ability for $H_2$ evolution.

### 3.3. Roles of rhodium and antimony species on photocatalytic properties of $SrTiO_3$:Rh/Sb

Effects of the Sb/Rh ratio on photocatalytic activities of $SrTiO_3$:Rh(2%)/Sb(Y%) for $H_2$ and $O_2$ evolution from aqueous solutions containing sacrificial reagents under visible light irradiation are shown in Table 1. The calcined sample with Sb/Rh = 0 showed the highest activity for the $H_2$ evolution although it could not oxidize water to form $O_2$ in the presence of $Ag^+$ ions as an electron acceptor. The activities for the $H_2$ evolution decreased as the

**Table 1**
Dependence of photocatalytic activities of $SrTiO_3$:Rh(2%)/Sb(Y%) for $H_2$ and $O_2$ evolution from aqueous solutions containing sacrificial reagents under visible-light irradiation on the Sb/Rh ratio.

| Sb/Rh ratio | Calcination[a] | $H_2$ reduction treatment[b] | Relative intensity of ESR signal related to $Rh^{4+}$ | Activity[c] ($\mu mol\ h^{-1}$) | | |
|---|---|---|---|---|---|---|
| | | | | $H_2$[d] | $O_2$[e] | |
| | | | | | Non-loaded | $IrO_x$-loaded[f] |
| 0 | Yes | No | 1.00 | 66 | 0 | 0 |
| 0 | Yes | Yes | 0.00 | 12 | 4 | 7 |
| 0.5 | Yes | No | 0.41 | 58 | 0 | 1 |
| 1.0 | Yes | No | 0.10 | 34 | 1 | 51 |
| 1.0 | No | No | – | 7 | 2 | 1 |
| 1.5 | Yes | No | 0.00 | 19 | 1 | 30 |

Catalyst, 0.2 g; light source, 300-W Xe lamp attached with cutoff filter; incident light, $\lambda > 420$ nm.
[a] 1273 K for 10 h.
[b] 673 K for 2 h.
[c] Initial rate.
[d] $H_2$ evolution: Pt cocatalyst (0.3 wt%), 150 mL of 10 vol% aqueous methanol solution.
[e] $O_2$ evolution: 150 mL of 0.02 mol $L^{-1}$ aqueous silver nitrate solution.
[f] 1.0 wt%.

amount of codoped antimony increased. In contrast, the activities for the $O_2$ evolution appeared by codoping of antimony. The highest activity was obtained in the sample with Sb/Rh = 1.0. The dependence of photocatalytic activities for the $O_2$ evolution on the Sb/Rh ratio was similar to those for $TiO_2$:Cr/Sb and $TiO_2$:Rh/Sb photocatalysts [21,30]. The optimum Sb/Rh ratio for the $H_2$ evolution was different from that for the $O_2$ evolution. This result indicated that dominant factors affecting the $H_2$ evolution were different from those for $O_2$ evolution. The non-calcined sample with Sb/Rh = 1.0 showed lower activities than the calcined sample for $H_2$ and $O_2$ evolution. This result indicates that high crystallinities obtained by the calcinations are indispensable for high photocatalytic activities for the $H_2$ and $O_2$ evolutions.

ESR and DRS analyses revealed that rhodium species doped into a $SrTiO_3$ host without codoping of Sb was a mixture of $Rh^{3+}$ and $Rh^{4+}$ ions as mentioned in Section 3.1. The analyses led the mechanism of photocatalytic $H_2$ evolution from an aqueous solution in the presence of methanol over the most active $SrTiO_3$:Rh/Sb with Sb/Rh = 0 under visible light irradiation as follows. $Rh^{3+}$ ions stabilized by oxygen defects and $Rh^{4+}$ ions formed by high-temperature calcination in air existed in the calcined sample with Sb/Rh = 0. There was an induction period that a photoreduction of doped $Rh^{4+}$ ions to $Rh^{3+}$ ions would proceed preferentially in the early stage of the $H_2$ evolution [28]. After the induction period, $H_2$ evolution proceeded steadily as shown in Fig. 5(A). In the steady state of the $H_2$ evolution reaction, the donor levels consisted of two-types of $Rh^{3+}$ ions. One was $Rh^{3+}$ ions stabilized by oxygen defects and the other was unstable $Rh^{3+}$ ions formed by photoreduction during the induction period. The unstable $Rh^{3+}$ ions were easily oxidized to $Rh^{4+}$ ions by the exposure to air [28]. Here, the relative intensity of ESR signal related to $Rh^{4+}$ was positively correlated with the photocatalytic activity of $SrTiO_3$:Rh/Sb for the $H_2$ evolution as shown in Table 1. Fig. 6 shows diffuse reflection spectra of Pt-loaded $SrTiO_3$:Rh(2%)/Sb(Y%) before and after the $H_2$ evolution. The visible light absorption bands around 580 nm involved with $Rh^{4+}$ ions were weakened after the $H_2$ evolution except for the sample of Sb/Rh = 1.5 in which no $Rh^{4+}$ ions were observed by ESR and DRS analyses as shown in Figs. 1 and 2. The decrease in this band of Sb/Rh = 0 was more remarkable than that of Sb/Rh = 1.0. Therefore, the smaller the amount of codoped antimony was, the larger the amount of unstable $Rh^{3+}$ ions was, resulting in the enhancement of photocatalytic activities for the $H_2$ evolution. This result indicated that the unstable $Rh^{3+}$ ions formed by the photoreduction of $Rh^{4+}$ ions were more effective for the $H_2$ evolution than the stabilized $Rh^{3+}$ ions by oxygen defects. This mechanism has been proposed in a previous paper [28]. In the present study, it was also confirmed by using $SrTiO_3$ photocatalysts codoped with rhodium and antimony. The difference in environments between the unstable $Rh^{3+}$ ions and the stabilized $Rh^{3+}$ ions is as follows. When $SrTiO_3$:Rh/Sb photocatalysts possessing $Rh^{4+}$ ions absorbed visible light, pairs of electrons and holes were generated. The holes were irreversibly consumed with oxidation of methanol, while the electrons reduced the electron-acceptable $Rh^{4+}$ ions to unstable $Rh^{3+}$ ions. The charge imbalance with the formation of unstable $Rh^{3+}$ ions would be compensated probably by adsorption of protons on the photocatalyst surface. Thus, as unstable $Rh^{3+}$ ions were hardly affected by oxygen defects which work as recombination centers, the lifetime of holes photogenerated in the donor levels consisting of unstable $Rh^{3+}$ ions prolonged, resulting in the high activity for the $H_2$ evolution. On the other hand, codoping of antimony could form $Rh^{3+}$ ions without the formation of oxygen defects. However, the substitution of antimony for titanium might disturb the conduction band consisting of $Ti^{4+}$ 3d orbitals. This should be a negative effect on photocatalytic performance of $SrTiO_3$:Rh/Sb photocatalyst especially for $H_2$ evolution from an aqueous methanol solution because the conduction band level is close to the potential for $H_2$ evolution (−0.2 V vs. NHE) and the activity should be sensitive to the character of the conduction band.

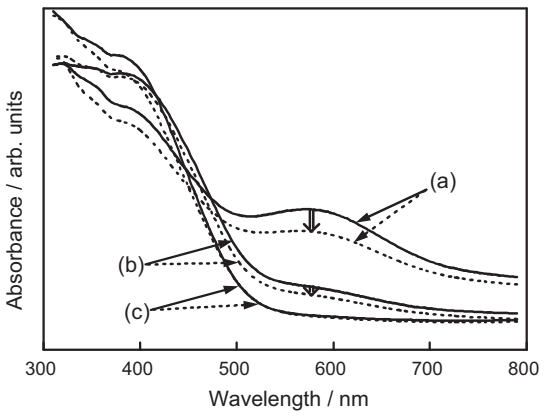


**Fig. 6.** Diffuse reflection spectra of Pt(0.3 wt%)/$SrTiO_3$:Rh/Sb before (solid line) and after (dot line) $H_2$ evolution under visible light irradiation. Sb/Rh ratios were (a) 0; (b) 1.0; and (c) 1.5. The amount of doped Rh was fixed at 2%. The bases of spectra were wholly raised by absorption of loaded Pt cocatalyst.

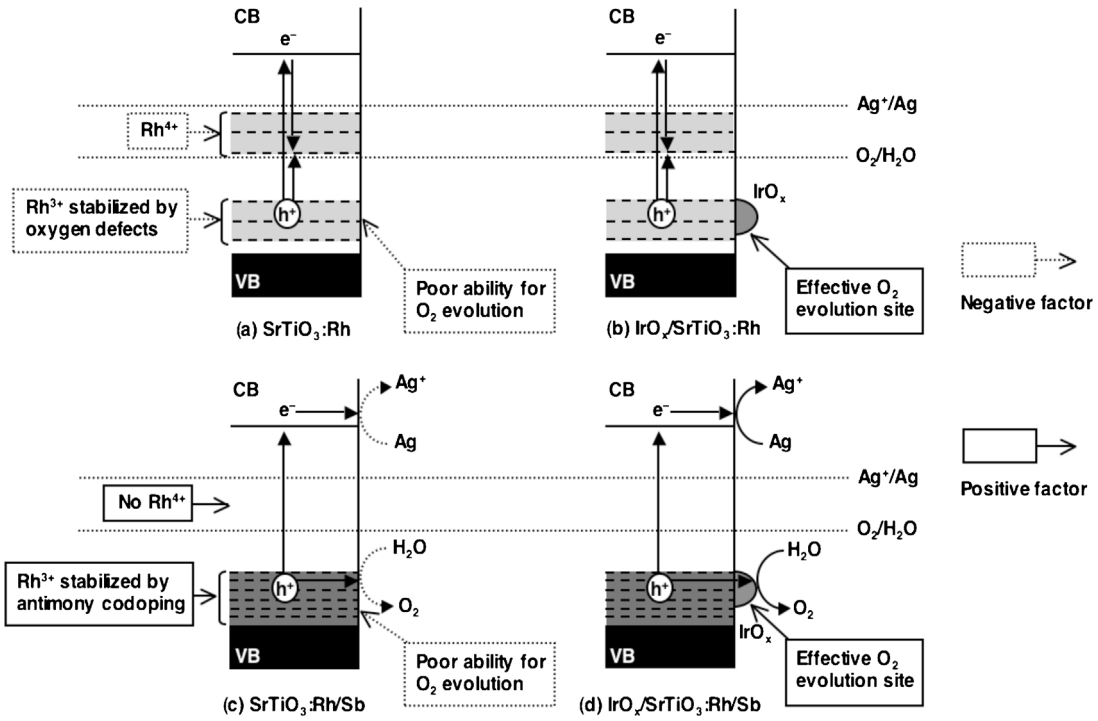


**Fig. 7.** Proposed scheme of photocatalytic $O_2$ evolution over $SrTiO_3$:Rh/Sb under visible light irradiation.

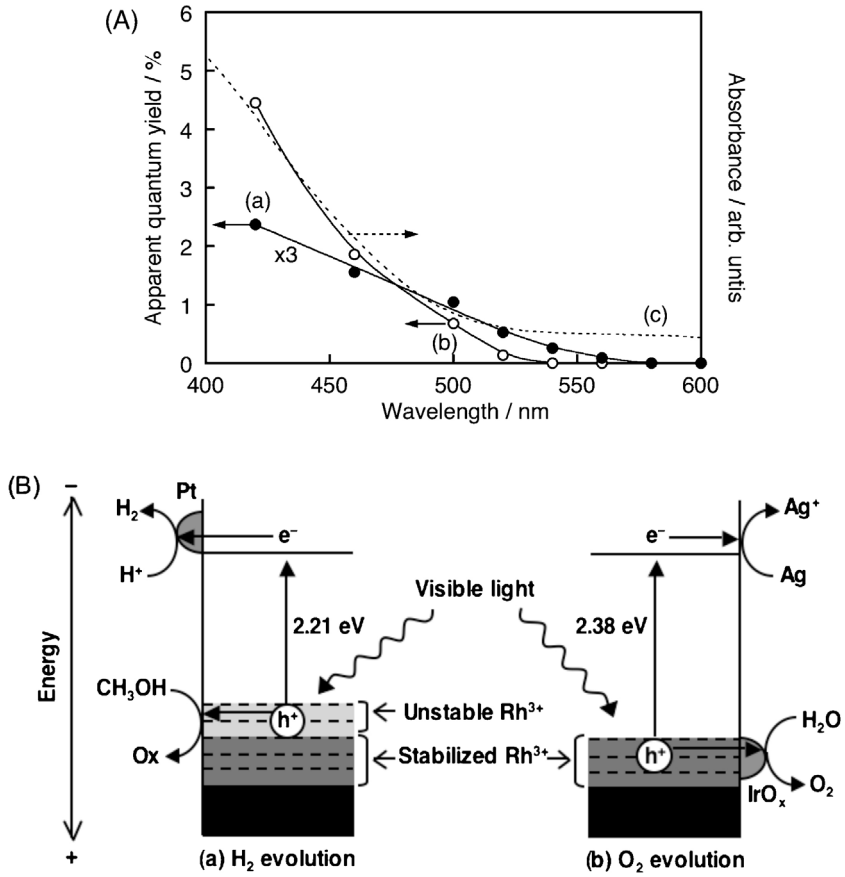


**Fig. 8.** (A) Action spectra for (a) $H_2$ and (b) $O_2$ evolution from aqueous solutions containing sacrificial reagents and (c) a diffuse reflection spectrum of $SrTiO_3$:Rh(1%)/Sb(1%). Catalyst, 0.2 g; $H_2$ evolution: 150 mL of 10 vol% aqueous methanol solution; Pt cocatalyst (0.3 wt%) was loaded, $O_2$ evolution: 150 mL of 0.02 mol $L^{-1}$ aqueous silver nitrate solution; $IrO_X$ cocatalyst (3.0 wt%) was loaded; light source, 300 W Xe lamp attached with band-pass filter. (B) Proposed mechanism for visible-light response of $SrTiO_3$:Rh/Sb photocatalyst.

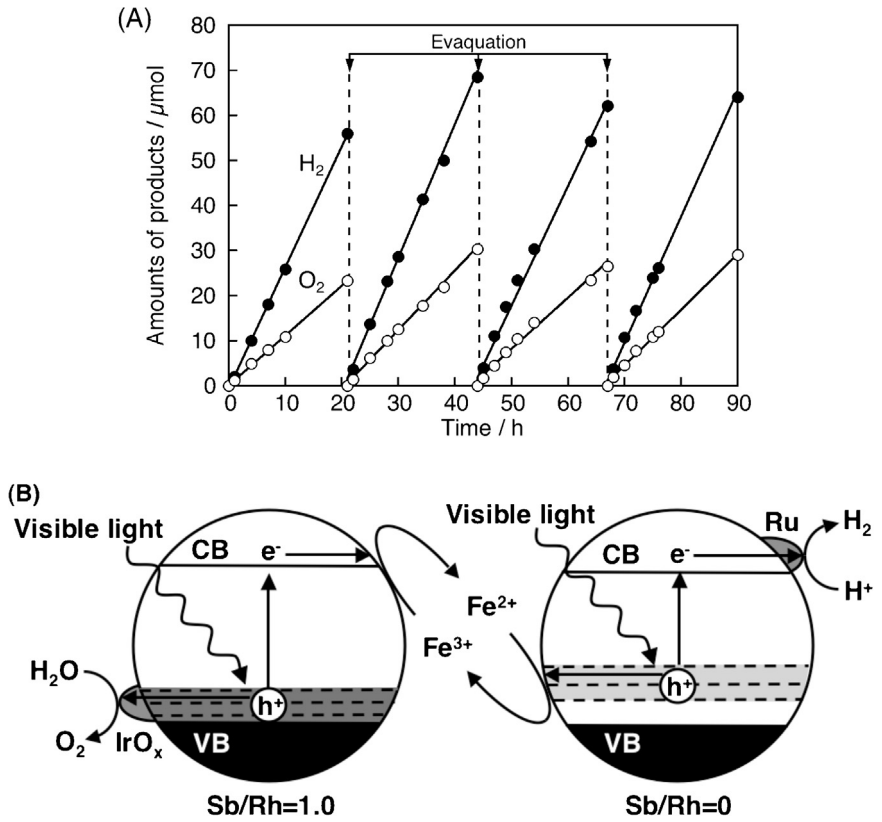


**Fig. 9.** (A) Photocatalytic overall water splitting under visible light irradiation by *Z*-scheme system. Catalyst, 50 mg of Ru(1.0 wt%)/$SrTiO_3$:Rh(2%) ($H_2$-evolving photocatalyst), and 50 mg of $IrO_X$(3.0 wt%)/$SrTiO_3$:Rh(1%)/Sb(1%) ($O_2$-evolving photocatalyst); reactant solution, 120 mL of 2 mmol $L^{-1}$ $Fe_2(SO_4)_3$ aqueous solution (pH = 2.4 adjusted by $H_2SO_4$); cell, top-irradiation type; light source, 300-W Xe lamp attached with cutoff filter; incident light, λ > 420 nm. (B) Mechanism for overall water splitting of *Z*-scheme system.

The results of Table 1 revealed important factors for $O_2$ evolution from an aqueous silver nitrate solution over $SrTiO_3$:Rh/Sb under visible light irradiation as shown in Fig. 7. The sample doped with only rhodium (Sb/Rh = 0) showed no photocatalytic activity for the $O_2$ evolution (Fig. 7(a)). Moreover, no enhancement was observed even by loading of $IrO_X$ cocatalyst (Fig. 7(b)). In the case of the $O_2$ evolution, the photoreduction of the electron-acceptable $Rh^{4+}$ ions did not proceed due to the absence of an electron donor such as methanol. In addition, the energy gap between a top of the valence band and a bottom of the electron accepter levels consisting of $Rh^{4+}$ ions was estimated to be ca. 1.6 eV from the onset of the visible light absorption peak around 580 nm (Fig. 2(B)). This observation indicated that the bottom of the electron acceptor levels was more positive than the redox potential of $Ag^+$/Ag (0.8 V vs. NHE) even around neutral pH. It resulted in that the electrons could not reduce $Ag^+$ to form metallic Ag even if electrons were produced in the electron acceptor levels with visible light excitation. The high-valent $Rh^{4+}$ ions merely work as recombination sites between photogenerated electrons and holes under such experimental condition. Thus, when only rhodium was doped into a $SrTiO_3$ host without codopant, large amounts of $Rh^{4+}$ ions were formed, resulting in no photocatalytic activity. On the other hand, in cases of the samples with Sb/Rh = 0.5, 1.0, and 1.5, even the sample of Sb/Rh = 1.5 in which there were only $Rh^{3+}$ ions stabilized by codoping of antimony hardly showed the photocatalytic activity for the $O_2$ evolution. This was due to that visible-light-sensitized $SrTiO_3$:Rh/Sb photocatalysts possessed surfaces with poor abilities for 4-electron oxidation of water to form $O_2$ (Fig. 7(c)), in contrast to rutile-type $TiO_2$ doped with rhodium and antimony [30]. When the surfaces of $SrTiO_3$:Rh/Sb photocatalysts were modified by loading of $IrO_X$ cocatalysts, the photocatalytic activities were drastically improved (Fig. 7(d)). The samples with Sb/Rh = 1.0 and 1.5 showed much higher activity than a $H_2$-treated sample with Sb/Rh = 0 because codoping of antimony could stabilize $Rh^{3+}$ ions toward oxidation without the formation of oxygen defects. The sample with Sb/Rh = 1.0 showed the highest activity among them, in spite of the existence of residual $Rh^{4+}$ ions as shown in Table 1. This result would be involved with the formation of $Sb^{3+}$ ions. $Sb^{3+}$ ions formed by self-charge compensation would cause $SrTiO_3$ lattice distortion that disturbed the migration of photogenerated carriers and worked as recombination centers, because of the large difference in the size between $Sb^{3+}$ (0.90 Å) and $Ti^{4+}$ (0.745 Å). The highest photocatalytic activity for the $O_2$ evolution was observed in the Sb/Rh = 1.0 due to the balance between the positive effect of the decrease in the amount of $Rh^{4+}$ ions and the negative effect of the formation of $Sb^{3+}$ ions. Thus, stabilization of $Rh^{3+}$ ions by codoping of antimony without oxygen defects and loading of $IrO_X$ cocatalyst were important for photocatalytic performance of $SrTiO_3$:Rh/Sb for the $O_2$ evolution under visible light irradiation.

Fig. 8(A) shows DRS of $SrTiO_3$:Rh(1%)/Sb(1%) and action spectra for $H_2$ and $O_2$ evolutions from aqueous solutions containing sacrificial reagents. The onsets of action spectra for $H_2$ and $O_2$ evolution almost agreed with that of a diffuse reflection spectrum. This result indicated that visible-light responses for both of the $H_2$ and $O_2$ evolutions were due to the electronic transition from the electron donor levels consisting of $Rh^{3+}$ 4d orbitals to the conduction band of $SrTiO_3$ host. However, photocatalytic activity for the $H_2$ evolution appeared at slightly longer wavelength (ca. 40 nm) than that for the $O_2$ evolution. Only $Rh^{3+}$ ions stabilized by codoping of antimony were active for $O_2$ evolution. In contrast, unstable $Rh^{3+}$ ions formed by photoreduction also worked for the $H_2$ evolution in addition to the stabilized $Rh^{3+}$ ions. The unstable $Rh^{3+}$

ions should possess higher electron-donating property than the stabilized $Rh^{3+}$ ions. Therefore, the unstable $Rh^{3+}$ ions formed an electron donor levels in more negative position than the stabilized $Rh^{3+}$ ions, resulting in the red shift of the action spectrum and the energy-gap narrowing as shown in Fig. 8(A) and (B), respectively. Their apparent quantum yields at 420 nm for the $H_2$ evolution over Pt(0.3 wt%)/$SrTiO_3$:Rh(1%)/Sb(1%) and $O_2$ evolution over $IrO_X$(3.0 wt%)/$SrTiO_3$:Rh(1%)/Sb(1%) were 0.8% and 4.5%, respectively. It is noteworthy that the $IrO_X$(3.0 wt%)/$SrTiO_3$:Rh(1%)/Sb(1%) photocatalyst showed the highest activity for $O_2$ evolution among metal cation-doped oxide photocatalysts. It was confirmed that if the stability of $Rh^{3+}$ ions toward oxidation was controlled by use of antimony codoping, rhodium-doped $SrTiO_3$ showed good photocatalytic performance for the $O_2$ evolution under visible light irradiation.

### 3.4. Construction of Z-scheme system for overall water splitting under visible light irradiation with two types of $SrTiO_3$:Rh/Sb photocatalysts

Two-types of $SrTiO_3$:Rh/Sb photocatalysts modified with appropriated cocatalysts were employed as $H_2$- and $O_2$-evolving photocatalysts, respectively, in order to construct a *Z*-scheme system using an $Fe^{3+}/Fe^{2+}$ redox couple as an electron mediator for overall water splitting under visible light irradiation. Ru cocatalyst was used for the $H_2$-evolving photocatalyst because backward reactions to form $H_2O$ from evolved $H_2$ and $O_2$ hardly proceeded on the surface [11]. $H_2$ and $O_2$ gases steadily evolved in a stoichiometric ratio ($H_2$:$O_2$ = 2:1) as shown in Fig. 9(A). The turnover numbers for the reacted electrons or holes to the amount of Fe ions (240 μmol) at 90 h of the overall water splitting reaction reached two. These results indicated that the overall water splitting reaction proceeded photocatalytically under visible light irradiation using the present *Z*-scheme system employing metal-doping photocatalysts as shown in Fig. 9(B).

## 4. Conclusions

$SrTiO_3$:Rh/Sb photocatalysts with visible-light responses for not only $H_2$ evolution but also $O_2$ evolution from aqueous solutions containing sacrificial reagents under visible light irradiation were successfully developed using a hydrothermal synthesis. Although visible-light responses of $SrTiO_3$:Rh/Sb for both of the $H_2$ and $O_2$ evolutions were due to the electronic transition from the electron donor levels consisting of $Rh^{3+}$ 4d orbitals to the conduction band, an effective rhodium species for the $H_2$ evolution was different from that for the $O_2$ evolution. The highest $H_2$ evolution activity was obtained for $SrTiO_3$ doped with only rhodium (Sb/Rh = 0). The unstable and reversible $Rh^{3+}$ ions in oxidation state that were formed by reduction by photoexcited electrons played an important role in the $H_2$ evolution under visible light irradiation. On the other hand, stabilizing the $Rh^{3+}$ ions by codoping of antimony without the formation of $Rh^{4+}$ ions and/or oxygen defects which worked as undesirable recombination sites was important for the $O_2$ evolution. The optimum Sb/Rh ratio was unity for the $O_2$ evolution. Systematic changes in ESR, DRS, and Raman spectra by codoping indicate that rhodium and antimony were doped in the lattice of $SrTiO_3$ host in the same particles using a hydrothermal synthesis, resulting in the efficient charge compensation. Loading of $IrO_X$ cocatalyst drastically improved the photocatalytic activity of $SrTiO_3$:Rh/Sb for the $O_2$ evolution. Overall water splitting under visible light irradiation was achieved by a *Z*-scheme system constructed of $SrTiO_3$:Rh/Sb photocatalysts with the Sb/Rh ratio of zero ($H_2$-evolving photocatalyst) and unity ($O_2$-evolving photocatalyst), and an $Fe^{3+}/Fe^{2+}$ redox couple (electron mediator). The present study revealed the importance of codoping technique for development of visible-light-driven photocatalysts doped with metal cations for $H_2$ and $O_2$ evolution and the possibility of the application of transition metal-doped photocatalysts with activities for half reaction of water splitting to overall water splitting.

## Acknowledgments

This work was supported by a Grant in Aid (No. 24107004) for Scientific Research on Innovative Areas (No. 2406) from the Ministry of Education, Culture, Sports, Science & Technology in Japan. The authors thank Dr. Iwase for his valuable discussion, and Mr. Jia, Mr. Asako and Ms. Motomura for help in some experiments.

## Appendix A. Supplementary data

Supplementary material related to this article can be found, in the online version, at http://dx.doi.org/10.1016/j.apcatb.2013.12.015.

## References

[1] K. Domen, J.N. Kondo, M. Hara, T. Takata, Bull. Chem. Soc. Jpn. 73 (2000) 1307–1331.
[2] K. Maeda, K. Domen, J. Phys. Chem. C 111 (2007) 7851–7861.
[3] F.E. Osterloh, Chem. Mater. 20 (2008) 35–54.
[4] A. Kudo, Y. Miseki, Chem. Soc. Rev. 38 (2009) 253–278.
[5] Y. Inoue, Energy Environ. Sci. 2 (2009) 364–386.
[6] K. Sayama, K. Mukasa, R. Abe, Y. Abe, H. Arakawa, Chem. Commun. (2001) 2416–2417.
[7] R. Abe, T. Takata, H. Sugihara, K. Domen, Chem. Commun. (2005) 3829–3831.
[8] K. Maeda, K. Teramura, D. Lu, T. Takata, N. Saito, Y. Inoue, K. Domen, Nature 440 (2006) 295.
[9] H. Kato, Y. Sasaki, A. Iwase, A. Kudo, Bull. Chem. Soc. Jpn. 80 (2007) 2457–2464.
[10] Y. Lee, H. Terashima, Y. Shimodaira, K. Teramura, M. Hara, H. Kobayashi, K. Domen, M. Yashima, J. Phys. Chem. C 111 (2007) 1042–1048.
[11] Y. Sasaki, A. Iwase, H. Kato, A. Kudo, J. Catal. 259 (2008) 133–137.
[12] M. Higashi, R. Abe, K. Teramura, T. Takata, B. Ohtani, K. Domen, Chem. Phys. Lett. 452 (2008) 120–123.
[13] Y. Sasaki, H. Nemoto, K. Saito, A. Kudo, J. Phys. Chem. C 113 (2009) 17536–17542.
[14] K. Maeda, M. Higashi, D. Lu, R. Abe, K. Domen, J. Am. Chem. Soc. 132 (2010) 5858–5868.
[15] A.A. Krasnovskii, G.P. Brin, Dokl. Akad. Nauk SSSR 147 (1962) 656–659.
[16] J.-F. Reber, K. Meier, J. Phys. Chem. 90 (1986) 824–834.
[17] Y. Sakata, T. Yamamoto, T. Okazaki, H. Imamura, S. Tsuchiya, Chem. Lett. (1998) 1253–1254.
[18] T. Ohno, F. Tanigawa, K. Fujihara, S. Izumi, M. Matsumura, J. Photochem. Photobiol., A 127 (1999) 107–110.
[19] A. Kudo, M. Sekizawa, Catal. Lett. 58 (1999) 241–243.
[20] A. Kudo, M. Sekizawa, Chem. Commun. (2000) 1371–1372.
[21] H. Kato, A. Kudo, J. Phys. Chem. B 106 (2002) 5029–5034.
[22] A. Ishikawa, T. Takata, J.N. Kondo, M. Hara, H. Kobayashi, K. Domen, J. Am. Chem. Soc. 124 (2002) 13547–13553.
[23] G. Hitoki, A. Ishikawa, T. Takata, J.N. Kondo, M. Hara, K. Domen, Chem. Lett. 31 (2002) 736–737.
[24] G. Hitoki, T. Takata, J.N. Kondo, M. Hara, H. Kobayashi, K. Domen, Chem. Commun. (2002) 1698–1699.
[25] I. Tsuji, A. Kudo, J. Photochem. Photobiol., A 156 (2003) 249–252.
[26] K. Nukumizu, J. Nunoshige, T. Takata, J.N. Kondo, M. Hara, H. Kobayashi, K. Domen, Chem. Lett. 32 (2003) 196–197.
[27] T. Ishii, H. Kato, A. Kudo, J. Photochem. Photobiol., A 163 (2004) 181–186.
[28] R. Konta, T. Ishii, H. Kato, A. Kudo, J. Phys. Chem. B 108 (2004) 8992–8995.
[29] R. Niishiro, H. Kato, A. Kudo, Phys. Chem. Chem. Phys. 7 (2005) 2241–2245.
[30] R. Niishiro, R. Konta, W.J. Chun, K. Asakura, A. Kudo, J. Phys. Chem. C 111 (2007) 17420–17426.
[31] Y. Shimodaira, H. Kato, H. Kobayashi, A. Kudo, Bull. Chem. Soc. Jpn. 80 (2007) 885–893.
[32] A. Iwase, K. Saito, A. Kudo, Bull. Chem. Soc. Jpn. 82 (2009) 514–518.
[33] X. Wang, K. Maeda, A. Thomas, K. Takanabe, G. Xin, M.J. Carlsson, K. Domen, Nat. Mater. 8 (2009) 76–80.
[34] Y. Miseki, H. Kusama, H. Sugihara, K. Sayama, J. Phys. Chem. Lett. 1 (2010) 1196–1200.
[35] Y. Miseki, A. Kudo, ChemSusChem 4 (2011) 245–251.
[36] B. Siritanaratkul, K. Maeda, T. Hisatomi, K. Domen, ChemSusChem 4 (2011) 74–78.
[37] F. Zhang, A. Yamakata, K. Maeda, Y. Moriya, T. Takata, J. Kubota, K. Teshima, S. Oishi, K. Domen, J. Am. Chem. Soc. 134 (2012) 8348–8351.
[38] Y. Lee, T. Watanabe, T. Takata, M. Hara, M. Yoshimura, K. Domen, Bull. Chem. Soc. Jpn. 80 (2007) 423–428.

[39] M. Yoshino, M. Kakihana, Chem. Mater. 14 (2002) 3369–3376.
[40] Y. Miseki, H. Kato, A. Kudo, Chem. Lett. 35 (2006) 1052–1053.
[41] A. Kudo, K. Ueda, H. Kato, Catal. Lett. 53 (1998) 229–230.
[42] A. Kudo, K. Omori, H. Kato, J. Am. Chem. Soc. 121 (1999) 11459–11467.
[43] S. Kawasaki, K. Akagi, K. Nakatsuji, S. Yamamoto, I. Matsuda, Y. Harada, J. Yoshinobu, F. Komori, R. Takahashi, M. Lippmaa, C. Sakai, H. Niwa, M. Oshima, K. Iwashina, A. Kudo, J. Phys. Chem. C 116 (2012) 24445–24448.
[44] W.G. Nilsen, J.G. Skinner, J. Chem. Phys. 48 (1968) 2240–2248.
[45] H. Zheng, I.M. Reaney, G.D.C. Csete de Györgyfalva, R. Ubic, J. Yarwood, M.P. Seabra, V.M. Ferreira, J. Mater. Res. 19 (2004) 488–495.
[46] R.D. Shannon, Acta Crystallogr. A 32 (1976) 751–767.
[47] A.A. Sirenko, I.A. Akimov, J.R. Fox, A.M. Clark, H.-C. Li, W. Si, X.X. Xi, Phys. Rev. Lett. 82 (1999) 4500–4503.
[48] T. Ikeda, T. Nomoto, K. Eda, Y. Mizutani, H. Kato, A. Kudo, H. Onishi, J. Phys. Chem. C 112 (2008) 1167–1173.
[49] A. Iwase, H. Kato, A. Kudo, Chem. Lett. 34 (2005) 946–947.
[50] Y. Hosogi, Y. Shimodaira, H. Kato, H. Kobayashi, A. Kudo, Chem. Mater. 20 (2008) 1299–1307.